# SYNCHROTRON BASED X-RAY ABSORPTION SPECTROSCOPY FOR STRUCTURAL ANALYSIS OF BASALT FIBERS

**LICHTENBERG, HENNING[1*]; MAHLTIG, BORIS[1]; KLYSUBUN, WANTANA[2]; PRANGE, ALEXANDER[1,3] AND HORMES, JOSEF[3,4]**

[1] Hochschule Niederrhein University of Applied Sciences, Reinarzstr. 49, D-47805 Krefeld, Germany
[2] Synchrotron Light Research Institute, 111 University Ave. Muang District, Nakhon Ratchasima 30000, Thailand
[3] Center for Advanced Microstructures and Devices, Louisiana State University, 6980 Jefferson Hwy., Baton Rouge LA 70806, USA
[4] Rheinische Friedrich-Wilhelm-University, Nussallee 12, D-53115 Bonn, Germany

## ABSTRACT

X-ray Absorption Near Edge Structure (XANES) spectroscopy at the Synchrotron Light Research Institute (Thailand) was used to investigate temperature related structural changes in basalt fibers. As a first step, XANES spectra of fiber samples cut from a basalt roving heated for 1 hour at 800 °C were recorded at the K absorption edges of three chemical elements and compared with the spectra of the untreated fibers. Silicon and calcium K-edge XANES spectra of the fibers were not affected by heating, whereas iron K-edge XANES spectra were significantly influenced by heating at 800 °C. The high iron content in basalt fibers has been attributed to their higher thermal stability compared to common natural or synthetic fibers. As a next step, iron K-edge XANES spectra of two types of fibers (basalt roving and uncoated chopped fibers) were recorded after heating at temperatures between 600 °C and 900 °C. In both cases, with increasing temperature the absorption edge shifts to higher energies, indicating progressing oxidation of the iron atoms in the fibers. These experiments demonstrate the potential of X-ray absorption spectroscopy as a powerful analytical tool to investigate structural changes in basalt fibers upon heating and to correlate them with changes in their mechanical properties.

## KEYWORDS

Basalt fibers; Thermal stability; Synchrotron; X-ray absorption spectroscopy.

## INTRODUCTION

Inorganic fiber materials are known for their high thermal stability even in presence of oxygen from air [1] [2]. To inorganic fibers, different types of fiber materials are counted, e.g. carbon fibers, glass fibers or ceramic fibers from oxidic or non-oxidic composition [3-6]. Glass fibers are built up by mixtures of amorphous inorganic oxides as silica and alumina [3]. There are also glass fibers with special properties available, as e.g. a special resistance against alkaline liquids [3] [4]. Such extraordinary properties are often directly connected to the special composition of these fibers. The mentioned alkaline resistance, for example, is related to the presence of zirconia as glass fiber component [4] [7]. In a certain way similar to glass fibers are basalt fibers. Basalt fibers consist of different inorganic oxides and are also X-ray amorphous. However, basalt fibers are produced from natural volcanic rocks, which are molten for fiber production by spinning [8-10]. The composition of basalt fibers is determined by the composition of the rocks originally used. Compared to conventional glass fibers, basalt fibers contain a significant amount of iron oxide, giving them a typical brown coloration. Basalt fibers also contain titania in certain amounts [10-13]. Of course, there are also bulk-glass materials available which contain iron oxides or other iron compounds – with the aim to realize colored glass products, as e.g. used as bottles for beer or red wine [14-16]. However, for glass fibers such compositions containing iron oxides are quite unusual, especially for industrial products. Due to their origin, basalt fibers are sometimes offered as kind of a natural product from volcanic stones. Compared to common natural or synthetic fibers, they exhibit higher thermal and chemical stability and are also used in fiber composite reinforcements [10] [17] [18]. Their main component is silica, followed by titania, alumina, and iron oxide. A protective effect against heat radiation has been attributed to the iron oxide content [13] [19]. In general, the thermal stability of basalt fiber has been attributed to its high iron content [12] [20], and related to the iron redox state, specifically the iron oxides ratio, in the fiber [21] [22]. Changes in the structure and mechanical

* **Corresponding author:** Lichtenberg H., e-mail: *Henning.Lichtenberg@hs-niederrhein.de*
*Received September 4, 2024; accepted September 16, 2024*

properties of industrially used basalt fibers caused by heating and chemical treatment with acidic and alkaline solutions were investigated earlier [23]. It was reported that temperature had a significant influence on the fibers´ strength, which slightly decreased at ~300 °C, and rapidly at ~480 °C, finally resulting in complete disintegration. It should be noted that the maximum temperature of usage of basalt fibers is often given in the temperature range between 700 °C to 900 °C depending on the type of material and reference [10]. However, even treatments of these fibers at lower temperatures can decrease their strength. In earlier investigations [23], scanning electron microscopy before and after different thermal treatments did not indicate changes in fiber morphology, whereas energy-dispersive spectroscopy (EDS) showed significant changes in surface composition (removal of carbon) even after moderate heating. These changes were related to the decrease in strength and partly attributed to decomposition of the sizing agents on the fiber surface, which were obviously burned away. These conclusions were in agreement with the results of thermogravimetric and calorimetric analyses, and similar effects leading to similar conclusions were observed after acidic and alkaline treatments. Besides these changes in surface properties at lower temperature it was expected that thermal treatment at higher temperature leads to a change in bulk structure by crystallization and further damage which could be controlled by doping with other elements (e.g. Zr) [19-21] [23-25]. X-ray absorption spectroscopy (XAS) is an element specific and nondestructive characterization method giving access to detailed information about the atomic environment of selected chemical elements in the sample [26] [27]. X-ray Absorption Near Edge Structure (XANES) spectra provide information about the oxidation state and coordination geometry of the absorber atoms, while from Extended X-ray Absorption Fine Structure (EXAFS) data structural parameters like interatomic distances, types of neighboring atoms and coordination numbers can be extracted [28]. Both EXAFS and XANES spectroscopy are well established and widely used analytical tools, covering a broad bandwidth of applications in diverse fields of research such as nanomaterials, biological, environmental and agricultural research, cultural heritage, mineralogy, geochemistry, biomedical applications, chemical engineering, catalysis, battery research and sensors [29-35]. In contrast to other characterization techniques, XAS is not limited to crystalline materials but also applicable to amorphous solids, liquids and gases without elaborate sample preparation. Due to the penetration strength of X-rays, XANES and EXAFS spectroscopy can be used for bulk analysis of solids and interfaces, and the measurements can be performed *in situ*, e.g. during heating or in reactive gas atmosphere. The objective of this study was to use XANES spectroscopy as characterization method complementary to commonly used (mostly surface sensitive) laboratory techniques to analyze structural changes in basalt fibers upon thermal treatment in order to gain further insights into the mechanisms leading to the fibers´ decreasing mechanical stability. The results obtained can serve as a basis for future *in situ* XAS studies (e.g. using heatable sample cells), and ultimately contribute to the development of modified basalt fibers with enhanced temperature stability. Since the basalt fibers were expected to be mostly X-ray amorphous, XAS was considered as the ideal analytical tool for these investigations. This study covered absorption edges of different chemical elements and therefore included XAS measurements in a broad photon energy range. Accordingly, a tunable and highly intense X-ray source covering a wide range of energies was required, which is only accessible at a synchrotron light source.

## EXPERIMENTAL SECTION

### Samples and sample preparation

For a first series of XANES measurements, ca. 15 mm long pieces of a basalt fiber were cut from a basalt roving supplied by Incotechnology GmbH (Pulheim, Germany, type A) and heated for 1 hour in a muffle furnace at 800 °C. Infrared and EDS spectra of this type have been reported earlier [36] [37]. X-ray absorption spectra of these samples were measured at the absorption edges of three different chemical elements (silicon, calcium and iron). The silicon and calcium K-edge XANES spectra of these samples were identical to those of the untreated fiber, whereas the iron K-edge spectra of heated and untreated fibers showed significant differences. Consequently, the iron K- absorption edge was selected for a more systematic XANES investigation: First, the fiber sample from the roving was heated also at 480 °C (based on [23]) for 1 hour, and measured at the iron K-edge. The absorption spectrum of this sample was identical with the spectrum of the untreated fibers. Therefore, as a next step, fibers were subjected to the temperature treatment shown in Fig. 1 in the furnace: A heating rate of 5 °C/min was applied, and four target temperatures defined (600 °C, 700 °C, 800 °C and 900 °C). Each time a target temperature was reached the temperature was kept constant for 1 hour, and immediately afterwards a certain portion of the fibers (sample 1 – 4 in Fig. 1) was removed from the oven and prepared for iron K-edge XANES measurements. The remaining fibers in the furnace were heated to the next target temperature (plateau). This procedure was later also applied to prepare a different set of samples (type B) from uncoated chopped fibers (UCF) supplied by the company Deutsche Basalt Faser GmbH (Sangerhausen, Germany) for iron K-edge XANES spectroscopy. The use of these fibers as coating additives was reported

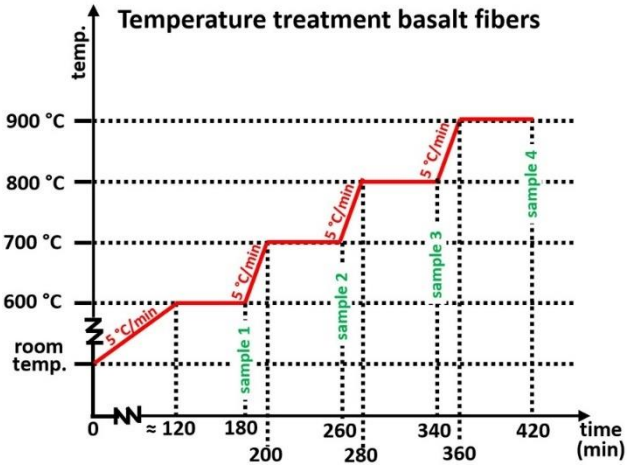


**Figure 1.** Temperature profile of temperature treatment applied to basalt fibers before iron K-edge XANES measurements.

earlier [38]. They were not cut, since they were already received chopped in ca. 0.5 cm long pieces. As expected, heating led to a clearly visible colour change in the fibers (from gold towards dark brown), which also became increasingly brittle.

For all XANES measurements, the fiber samples (either untreated or after heating) were on one side fixed with self-adhesive Kapton tape on a teflon sample holder, and on the opposite side (facing the beam) covered with polypropylene foil.

## XANES measurements

XANES spectra of the basalt fibers were recorded at beamline BL8 [39-41] at the Synchrotron Light Research Institute (SLRI, Thailand, Siam Photon Source, 1.2 GeV electron storage ring) using bending magnet radiation. The chemical composition of basalt rock, glasses and fibers is well known from numerous publications [12] [17] [20] [42-46]: $SiO_2$ clearly dominates (in terms of mass fraction between ca. 40 and 60 wt.%), followed by $Al_2O_3$, iron oxides (FeO, $Fe_2O_3$), CaO, MgO, $Na_2O$, $TiO_2$ and $K_2O$. The values for the mass fraction for the individual components vary from publication to publication by a few percent, probably to a great extent due to the different origins of the basalt samples investigated. For this XANES study, the three chemical elements with the highest reported mass fraction (in wt.%) and K absorption edges in the X-ray energy range between 1.8 keV and 10 keV were chosen: Silicon, calcium and iron. XANES spectroscopy at energies below 1.8 keV is generally also possible at beamline BL8 (down to ca. 1 keV, i.e. covering the absorption edges of aluminum, magnesium and sodium), however, such experiments are quite challenging (require rather uncommon monochromator crystals and thin foils as window and sample support materials) and will therefore be part of future studies.

For this project, the double crystal monochromator at BL8 was equipped with either InSb(111) crystals (for spectroscopy at the silicon K-edge, 1839 eV) or Ge(220) crystals (calcium and iron K-edge at 4039 eV and 7112 eV, respectively). The scan parameters for the measurements at these absorption edges are shown in table 1. The beamsize at the sample position was 10 mm x 1 mm. During XANES measurements the incident and transmitted monochromatic X-ray intensities were measured with ionization chambers, and the intensities of the $K_\alpha$ X-ray fluorescence lines of silicon, calcium and iron (at 1.74 keV, 3.69 keV and 6.41 keV) were measured with a 13-element germanium detector (Canberra) or a 7-element silicon drift detector (SGX Sensortech) positioned perpendicular to the beam direction in the plane of the beam. Fiber samples were oriented at 45° to the incident beam. During the measurements at the Si and Ca K absorption edge, the sample chamber was flushed with helium to minimize the attenuation of the fluorescence radiation by ambient air. All fiber samples were measured in fluorescence mode. For energy calibration of the monochromator, absorption spectra of silicon powder, calcium carbonate powder ($CaCO_3$) and an iron foil were recorded in transmission mode. The first maximum of the first derivative of the Si powder spectrum was set to an energy of 1839 eV. For calibration at the calcium K-edge the first resonance (´white line´, absolute maximum) in the XANES spectrum of the $CaCO_3$ reference sample was set to an energy of 4049 eV.

To calibrate the set-up for iron K-edge spectroscopy the first maximum of the first derivative of the Fe foil spectrum was set to an energy of 7112 eV. XANES spectra (absorption coefficient as function of the photon energy E, in arbitrary units) were extracted from the raw data by background subtraction and normalization (and averaging over several spectra in cases where more than one XANES spectrum of the same sample was measured) using the Athena program [47].

## RESULTS AND DISCUSSION

### X-ray absorption near edge spectra at the K absorption edges of silicon, calcium and iron

Fig. 2 (a) shows silicon K-edge XANES spectra of untreated basalt fibers cut from the roving (type A) along with the spectra of the same fiber type heated for 1 hour at 800 °C. These spectra do not indicate any influence of this thermal treatment on the absorption behavior of silicon in these fibers. For comparison, a silicon K-edge XANES spectrum of quartz powder, measured on self-adhesive Kapton tape in transmission mode, is shown in Fig. 2 (b). The spectra of the basalt fibers and the quartz reference both show a pronounced absorption maximum („white line") at 1847 eV (1s → 3p transition [48-50]) and a broader „shape resonance" at ca. 1864 eV. Between these two spectral features, three additional absorption maxima appear in the quartz spectrum,

**Table 1.** Scan parameters for XANES measurements at different absorption edges.

| Edge | Energy range (step size) | | | Integration time |
|---|---|---|---|---|
| | ***Pre-edge region*** | ***Near edge region*** | ***Post-edge region*** | |
| Si K | 1789 - 1819 eV (3 eV) | 1819 - 1909 eV (0.2 eV) | 1909 - 1939 eV (3 eV) | 1 s |
| Ca K | 3950 - 4020 eV (2 eV) | 4020 - 4120 eV (0.2 eV) | 4120 - 4200 eV (1 eV) | 3 s |
| Fe K | 7000 - 7100 eV (2 eV) | 7100 - 7160 eV (0.5 eV) | 7160 - 7300 eV (1 eV) | 3 s |

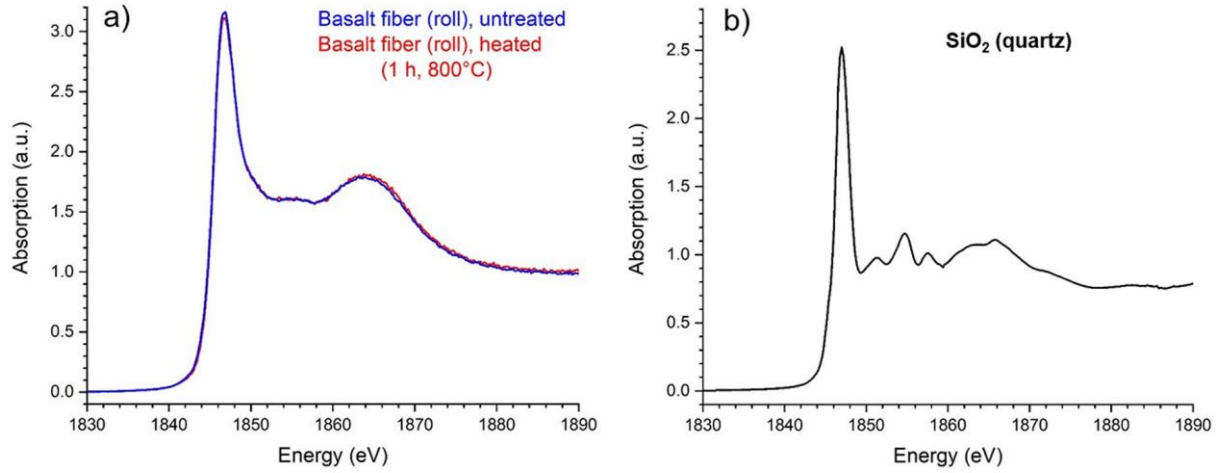


**Figure 2.** Silicon K-edge XANES spectra of: (a) basalt fibers cut from a roving (type A, ´roll´) and (b) CaO powder.

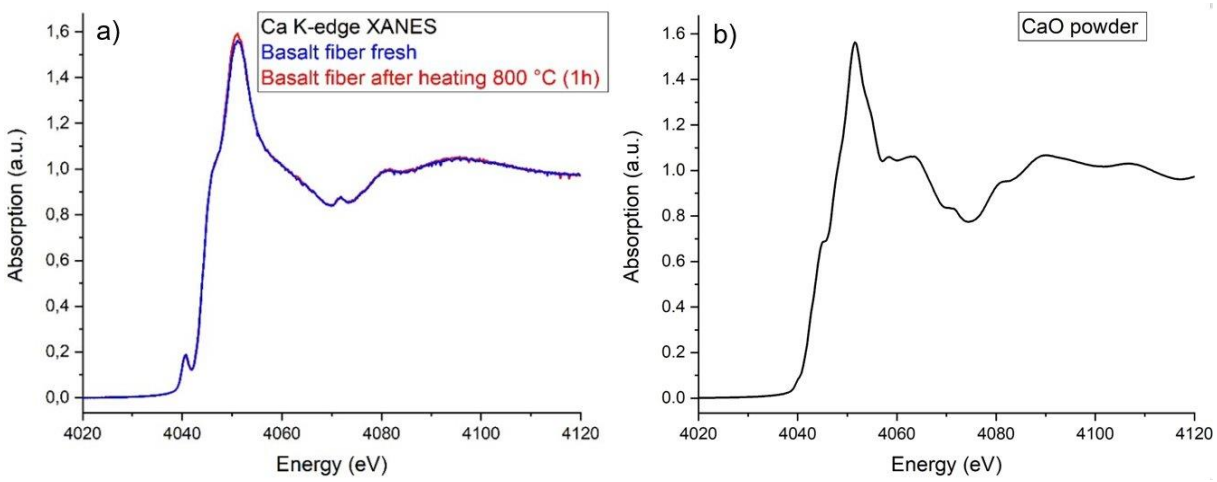


**Figure 3.** Calcium K-edge XANES spectra of: (a) basalt fibers cut from a roving (type A) and (b) quartz powder.

which are well known in the literature [48] and have been assigned by Li et al. [49] [50] to electronic transitions (1s → 3d/p) and multiple scattering processes. In the silicon K-edge absorption spectra of other stable crystalline modifications of $SiO_2$ like coesite and cristobalite, weak but clearly pronounced characteristic local absorption maxima above the white line are visible as well [48] [51-53].

In contrast, in the spectra of the basalt fibers (Fig. 2(a)) such features are not observed. In general, in amorphous $SiO_2$ they are suppressed in intensity and the absorption spectra are generally more diffuse due to the inherent disordered nature of such materials, featuring a broad range of Si-O-Si angles and Si-O and Si-Si distances compared to their crystalline counterparts [48] [54-57]. Accordingly, the spectra in Fig. 2(a) indicate an atomic environment of silicon very similar to amorphous $SiO_2$, as expected: Such basalt fibers are produced by melting basalt rocks between ca. 1400 °C and 1700 °C [13] [58], followed by rapid cooling causing the basalt to solidify in a glass-like amorphous phase [59]. From Fig. 2(a) it is obvious that the thermal treatment does not cause any distinct spectral features to emerge in the energy range between 1847 eV and 1864 eV. Accordingly, these measurements do not indicate crystallization of $SiO_2$ upon heating at 800 °C for one hour.

Fig. 3(a) shows calcium K-edge XANES spectra of the same fiber type (roving, type A), untreated and after one hour of heating at 800 °C. In most publications providing tabulated values for the chemical composition of basalt, the calcium

containing component is listed as “CaO”. A spectrum of CaO powder, measured on self-adhesive Kapton tape in transmission mode, is therefore shown in Fig. 3(b) for comparison. However, it clearly differs from the calcium K-edge spectra of the basalt fibers. Intensity, energy position and shape of the white line peak are roughly comparable (in both cases with a shoulder on the low energy side), but the basalt spectrum features a pronounced pre-edge resonance at ca. 4040 eV that does not appear in the CaO spectrum. On the other hand, above the white line two less intense peaks at 4059 eV and 4063 eV are observed in the CaO spectrum, but not in the absorption data of the fibers (assignment of absorption peaks in [48]). The spectra of the basalt fibers in Fig. 3(a) almost perfectly match several Ca k-edge XANES spectra of soda lime aluminosilicate glasses, which Cormier and Neuville compared with those of several Ca-bearing minerals [60]. The spectra of these crystalline references showed some additional features above the white line which were smoothed in the glass (except a weak local absorption maximum at ca. 4070 eV which occurs in most published Ca K-edge XANES spectra without physical interpretation). Occurrence and intensities of pre-edge features, which depend on the Ca site geometry (symmetry), varied from mineral to mineral. The comparatively high intensity of the pre-edge peak in the glasses was interpreted as an indication that the Ca environment is more distorted. The spectra of the basalt fibers in Fig. 3(a) also almost perfectly match the majority of XANES spectra of calcium aluminosilicate glasses [61], $CO_2$-bearing silicate glasses [62] and amorphous calcium silicate hydrates [63]. Moreover, the spectra of the basalt fibers in Fig. 3(a) resemble (although not as closely as the glasses mentioned above) the Ca K-edge XANES spectra of amorphous calcium carbonate which Brinza et al. [64] compared with spectra of the crystalline calcium carbonate phases calcite, aragonite and vaterite. In the post edge region (above the white line) these three crystalline references featured further absorption peaks and shoulders, whereas the amorphous calcium carbonate showed a smooth, relatively featureless decline from the white line to ca. 4068 eV. Qualitatively similar comparisons of amorphous and crystalline $CaCO_3$ polymorphs have been published by Kathyola et al. [65], Monico et al. [66] and Xto et al. [67], and also by Levi-Kalisman et al. [68] [69] and Lam et al. [70], who suggested an increase in structural disorder as a possible explanation for the observed decrease in the number of spectral features and their intensities in the post-edge regions of spectra when moving from the crystalline to the amorphous materials. Therefore, like the Si K-edge spectra in Fig. 2(a), the Ca K-edge spectra of the basalt fiber in Fig. 3(a) can be regarded as characteristic of a predominantly amorphous environment of the Ca or Si absorber atoms, which is not measurably affected by heating for 1 hour at 800 °C.

Fig. 4(a) shows iron K-edge XANES spectra of the same fiber type (roving, type A), untreated and after heating for one hour at 480 °C and 800 °C. For comparison, transmission mode iron K-edge XANES spectra of reference compounds with iron in different oxidation states (powders spread on self-adhesive Kapton tape) are shown in Fig. 4(b). These reference spectra show that with increasing oxidation number of iron the rising edge of the white line in the absorption spectra is shifted to higher energies. The spectra in Fig. 4(a) indicate that moderate heating for one hour at 480 °C does not have a measurable impact on the iron speciation in the fibers, whereas heating at 800 °C leads to significant changes in the spectra: The intensity of the white line increases, and its rising edge is shifted to higher energies by ca. 2 eV, indicating oxidation of the iron atoms. Similar results are reported for iron K-edge XANES studies on bulk glass samples containing iron oxide and bulk basalt samples [71] [72]. Referring to an earlier investigation, changes in the bulk structure of basalt fibers upon heating at higher temperature are interpreted as result of crystallization processes [19-21] [23-25]. Based on the silicon and calcium absorption data shown in Fig. 2 and Fig. 3, there is no indication of crystallization of the fibers – at least not at the applied temperature (max. 800 °C) and the relatively short duration of heating. Earlier studies indicate that upon moderate heating predominantly the carbon containing sizing agent is pyrolyzed [23].

This effect on the sizing agent is probably not reflected in the spectra in Fig. 4(a), since XANES in the here applied fluorescence mode is not a surface sensitive technique, and the carbon absorption edge lies far below the operating range of the beamline. In the future such processes could be investigated using surface sensitive X-ray absorption spectroscopy, e.g. in electron yield mode, like in general the chemical bonds between the sizing and the basalt fiber.

Unfortunately, a quantitative analysis of the basalt fiber Fe-K-XANES spectra by fitting them to a linear combination of reference spectra was not possible with the reference compounds measured so far (iron foil and iron oxide powders), even when FeO reference spectra from a data base were included as representatives of divalent iron (not shown). This is obviously due to the complexity of the basalt fiber with its amorphous and multicomponent nature. In the future, further candidates for suitable reference compounds, including minerals and amorphous materials, will be tested in order to properly identify the chemical speciation of iron in the untreated and heated fibers. In any case, it can be assumed that the iron atoms in the basalt fibers are already in an “oxidized state” before the thermal treatment, and heating leads to further oxidation, probably through a change in the ratio of trivalent iron and the total iron content.

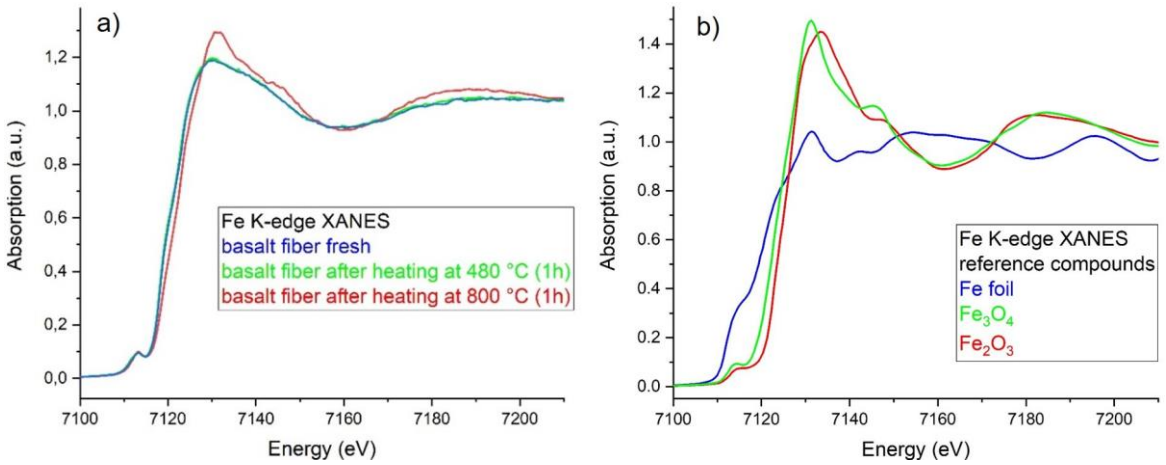


**Figure 4.** Iron K-edge XANES spectra of: (a) basalt fibers cut from a roving (type A) and (b) reference compounds.

## Further investigation of temperature influence on iron atoms in the fibers

Since heating at 800 °C did not affect the silicon and calcium K-edge XANES spectra measured so far, and heating at 480 °C did not influence the X-ray absorption of iron atoms in the basalt fibers, focusing on the iron K- absorption edge and setting the first target temperature of the furnace to 600 °C seemed a reasonable starting point for further experiments. Of course, these first measurements cannot reveal to which extent, besides the applied temperature, the duration of heating affects structural changes measurable through XANES (i.e. whether longer heating can have the same effect as increasing the temperature).

Fig. 5 shows iron K-edge XANES spectra of the basalt fibers cut from the roving (type A) which were thermally treated according to the temperature profile in Fig. 1. Increasing temperature (and heating time in the furnace) causes an increase in white line intensity along with a shift of the rising edge of the white line towards higher energies in the spectra, indicating progressing (further) oxidation of the iron atoms. The most pronounced differences occur between the spectra of samples heated up to 600 °C and those heated up to 800 °C. It is not yet clear to which final state the fiber is oxidized at the end of the procedure and whether the oxidation is accompanied by crystallization (results shown in Fig. 2 and Fig. 3 suggest that this does not occur up to at least 800 °C). Given the penetration strength of X-rays, one can assume that this oxidation occurs in the bulk material and not predominantly at the surface of the fibers.

For comparison, a second type of basalt fiber (uncoated chopped fibers, type B) was subjected to the same thermal treatment (Fig. 1). The iron K-edge XANES spectra of these samples are shown in Fig. 6. The changes in the spectra as a result of heating to different temperatures are similar to the observed changes in absorption behavior of the fiber samples from the roving: With increasing maximum heating temperature the rising edge of the white line in the spectra is shifted to higher energies while the white line intensity increases. Interestingly, in contrast to the fiber from the roving, in the spectra of the uncoated chopped fiber (Fig. 6) also the weak pre-edge feature at 7114 eV seems to be affected by the thermal treatment (maximum of pre-edge peak shifted by ca. 0.7 eV when moving from maximum temperature 600 °C to maximum temperature 700 °C). Analysis of pre-edge peaks in iron K-edge XANES spectra, which are due to 1s→3d transitions, has been used to determine oxidation state ($Fe^{2+}$ to $Fe^{3+}$ ratio) and coordination of iron in different materials [48] [73-75]. Whether the pre-edge shift in Fig. 6 is really caused by structural changes or an artefact due to a shift in the monochromator´s energy calibration needs to be carefully investigated.

In Fig. 7 iron K-edge XANES spectra of both fiber types A and B (roving and uncoated chopped fibers), subjected to the thermal treatment shown in Fig. 1, are directly compared (same data as in Fig. 5/6). In the ´fresh´ state and after being heated at 600 °C both fibers show the same absorption behavior: The spectra in Fig. 7(a) and (b) are identical within the noise level of the measurements. These results indicate that the atomic environment of the iron atoms in both types of fibers is very similar in this temperature range. After heating at 700 °C and 800 °C (spectra after heating at 900 °C not shown) the absorption behavior of the two fibers is different (Fig. 7 (c-d)): In the spectra of the uncoated chopped fiber (type B) the white line is more intense and the rising edge of the white line at higher energies compared to type A. However, based on these first results one should not jump to the conclusion that in this temperature range the iron atoms in the uncoated chopped fibers are more susceptible to (further) oxidation compared to fiber samples cut from the roving. Such conclusions, especially when based on relatively small differences the spectra of both fiber types (Fig. 7(c) and (d)), would require that the

thermal treatment for both fibers was exactly identical. This

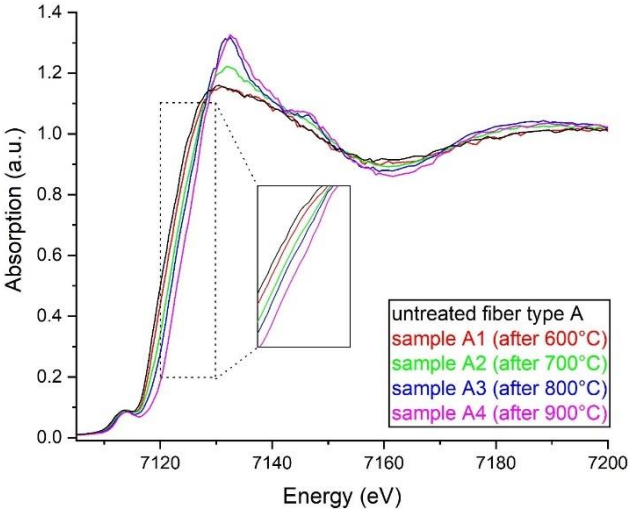


**Figure 5.** Iron K-edge XANES spectra of basalt fibers from the roving (type A) heated at different temperatures according to the temperature profile in Fig. 1.

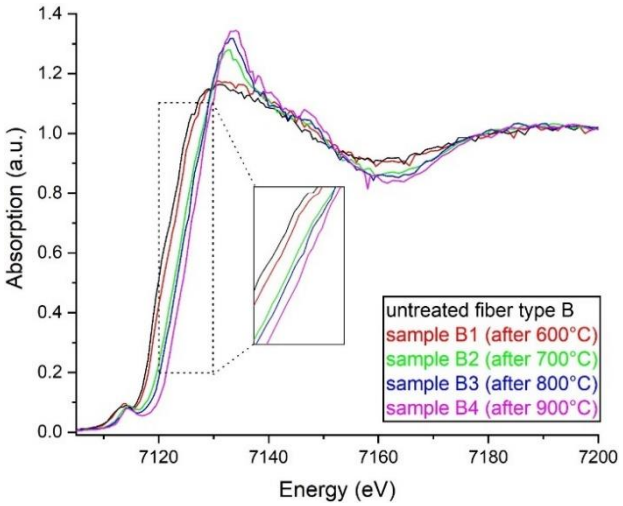


**Figure 6.** Iron K-edge XANES spectra of uncoated chopped basalt fibers (type B) heated at different temperatures according to the temperature profile in Fig. 1.

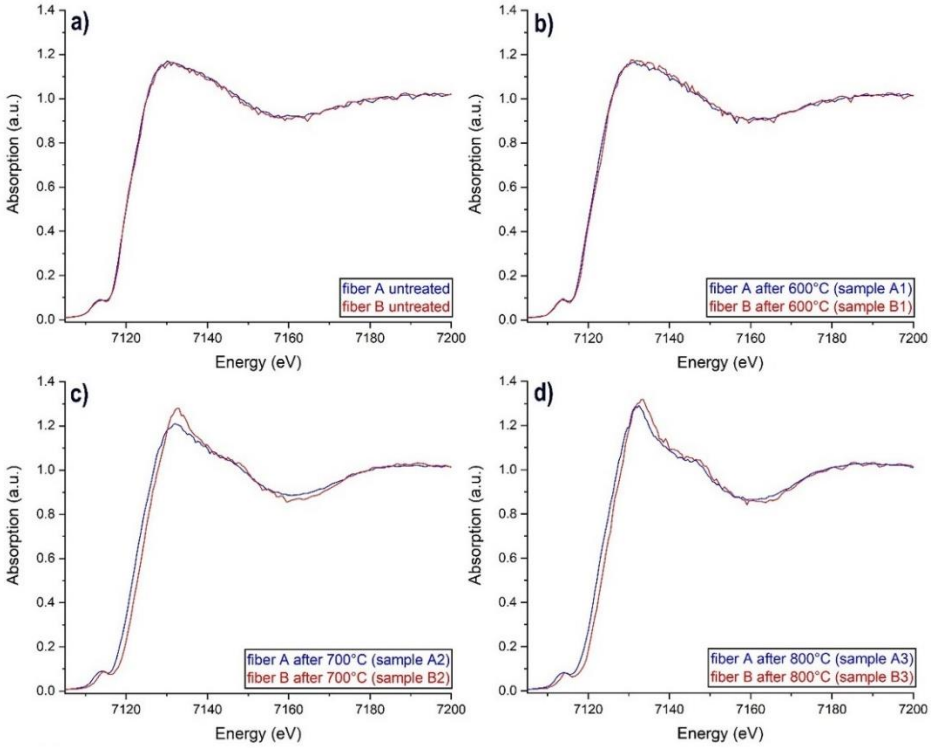


**Figure 7.** Iron K-edge XANES spectra: Comparison of two types of basalt fiber (type A: fiber samples cut from roving, type B: uncoated chopped fibers) heated to different maximum temperatures: (a) untreated, (b) 600 °C, (c) 700 °C, (d) 800 °C.

condition is not strictly fulfilled: The uncoated chopped fibers were heated after the XANES spectra of the thermally treated samples from the roving were recorded. Therefore, when preparing samples for future experiments the different types of fiber to be compared should be heated together in the furnace for better comparability. Further parameters to be taken into account for a comparison are potential differences in the physical properties of the fibers (e.g. diameter, density), and in the chemical composition.

## SUMMARY AND OUTLOOK

These XANES measurements show how X-ray absorption spectroscopy can be used to investigate structural changes in basalt fibers resulting from heating. As a first step, the K- absorption edges of silicon, calcium and iron were selected for recording XANES spectra of basalt fiber samples, which were cut from a roving and then heated for one hour at either 480 °C or 800 °C. The silicon and calcium K-edge spectra indicate an amorphous structure in the

basalt fibers. Since these spectra were not influenced by heating, there is no sign of crystallization at temperatures up to 800 °C during this, relatively short, duration of the thermal treatment. In contrast, the iron K-edge spectra of heated fibers showed significant differences compared to the untreated fibers, indicating a progressing oxidation of the iron atoms somewhere above 480 °C. The results suggest that the atomic environment of at least one chemical element (iron) in the fibers changes upon heating above a specific temperature, while other chemical elements (here silicon and calcium) apparently remain unaffected by thermal treatment – at least when heated at 800 °C for one hour. As a next step, the furnace used for sample preparation was programmed to ramp up the temperature to four target values between 600 °C and 900 °C and keep it constant at these points for one hour before proceeding to the next target temperature. After each temperature plateau, portions of fiber samples were taken from the furnace for iron K-edge XANES measurements. This thermal treatment was also applied to uncoated chopped fibers. In general, iron K-edge XANES spectra of both types of fibers show an increase in white line intensity and a shift of the rising edge of the white line towards higher energies with increasing maximum temperature. This shift can be attributed to a progressing oxidation of the iron atoms, the majority of which was most likely already in an oxidized state before heating. The thermal treatment then obviously leads to an increase in the relative concentration of trivalent iron compared to iron species with lower oxidation numbers. Small differences between the iron K-edge XANES spectra of the two fiber types heated at a maximum temperature above 600 °C may potentially indicate a higher susceptibility of the uncoated chopped fibers to oxidation compared to the fiber samples cut from the roving. However, a verifiable statement in this direction requires further systematic investigations, making sure that the two types of fiber were exposed to an identical thermal treatment, and considering their physical properties and chemical composition.

The results of this study demonstrate the high potential of XANES spectroscopy for the characterization of basalt fibers and their structural changes during heating, opening new perspectives in this field of research, especially when more systematic XANES studies are performed and extended to include further chemical elements in the fibers, or when set-ups for *in situ* X-ray absorption spectroscopy (with heatable sample cells) are used in order to correlate the spectroscopic data with temperature related changes in the mechanical properties of the fibers for a knowledge based development of modified basalt fibers with enhanced temperature stability (e.g. by surface treatment or doping with other chemical elements). However, the results of this first series of experiments leave some questions open for future studies under improved experimental conditions: The thermal treatment applied to the basalt fibers prior to the XANES measurements seemed to be the most practicable procedure for sample preparation at the beginning of the project. However, when following this protocol, a sample heated up to a specific maximum temperature was prior to reaching that specific target temperature already heated during ramping up from room temperature and in most cases (except the maximum 600 °C samples) also exposed to one hour heating at each lower temperature plateau. For future experiments one should invest more time in sample preparation, prepare separate batches of fibers to be heated at only one specific constant temperature for a specific time and wait each time until the furnace has reached this target temperature before placing the batch in it. On the other hand, different types of fibers to be compared later based on their XANES data should be placed in the furnace together to make sure that they were subjected to identical heating conditions for better comparability. The initial structure of the fibers before the thermal treatment could not be identified based on the data recorded so far, since this requires XANES spectra of special reference compounds beyond the ´standard´ oxide powders commonly used for quantitative analysis. Suitable reference compounds to be acquired for such studies should be as similar as possible to the basalt fibers´ (amorphous) structure and chemical/mineral composition. The data recorded so far do not provide information about processes on the fibers´ surface, since ´standard´ fluorescence mode XANES spectroscopy is not a surface sensitive technique. Moreover, it is not yet clear to which extent the observed oxidation of iron species is accompanied by crystallization. This could be investigated by powder X-ray diffraction or Extended X-ray Absorption Fine Structure (EXAFS) spectroscopy. Crystallization should result in more pronounced EXAFS oscillations with stronger contributions of higher coordination shells compared to the amorphous phase.

**Acknowledgement**: *This project was supported within the grant „Innovative Hochschule – Leuchtturm NR - Aus der Höhe in die Breite“ (03-IHS-084) by the Federal Ministry of Education and Research (Germany) and the EU Horizon2020 program (952148-Sylinda).*

## REFERENCES

1. Cooke T.F.: Inorganic fibers - a literature review, J. Am. Ceram. Soc. 74(12), 1991, pp. 2959-2978. https://doi.org/10.1111/j.1151-2916.1991.tb04289.x
2. Mahltig B.: Introduction to inorganic fibers. Book chapter in: Inorganic and composite fibers, Mahltig B., Kyosev Y. (Eds.) Woodhead Publishing – Elsevier, Duxford, UK, 2018, pp. 1-30.
3. Teschner R.: Glasfasern, Springer-Vieweg, Berlin, 2019, 2nd Edition.
4. Pico D., Wilms C., Seide G., et al.: Natural volcanic rock fibers, Chem. Fibers Int. 61(2), 2011, pp. 90-92.
5. Schawaller D., Clauß B., Buchmeiser M.R.: Ceramic filament fibers–a review, Macromol. Mater. Eng. 297(6), 2012, pp. 502-522.

https://doi.org/10.1002/mame.201100364
6. Mahltig B., Kyosev Y.: Inorganic and composite fibers, Woodhead Publishing – Elsevier, Duxford, UK, 2018
7. Ylmaz V.T., Lachowski E.E., Glasser F.P.: Chemical and microstructural changes at alkali‐resistant glass fiber‐cement interfaces, J. Am. Ceram. Soc. 74(12), 1991, pp. 3054-3060. https://doi.org/10.1111/j.1151-2916.1991.tb04301.x
8. Kumbhar V.P.: An overview: basalt rock fibers-new construction material, Acta Eng. Intl. 2(1), 2014, pp. 11-18.
9. Ivanitskii S.G., Gorbachev G.F.: Continuous basalt fibers: production aspects and simulation of forming processes I: State of the art in continuous basalt fiber technologies, Powder Metall. Met. C+ 50(3), 2011, pp. 125-129. https://doi.org/10.1007/s11106-011-9309-x
10. Mahltig B., Kyosev Y. (ed.): Basalt fibers, Book chapter in: Inorganic and composite fibers, Woodhead Publishing – Elsevier, Duxford, UK, 2018, pp. 195-218.
11. Ding L., Liu Y., Liu J., et al.: Correlation analysis of tensile strength and chemical composition of basalt fiber roving, Polym. Composite. 40(7), 2019, pp. 2959-2966. https://doi.org/10.1002/pc.25138
12. Deák T., Czigány T.: Chemical composition and mechanical properties of basalt and glass fibers: a comparison. Textile Res. J. 2009, 79(7), pp. 645-651. https://doi.org/10.1177/0040517508095597
13. Jamshaid H., Mishra R.: A green material from rock: basalt fiber – a review, J. Text. I. 107(7), 2016, pp. 923-937. https://doi.org/10.1080/00405000.2015.1071940
14. Donald S.B., Swink A.M., Schreiber H.D.: High-iron ferric glass, J. Non-Cryst. Solids 352(6-7), 2006, pp. 539-543. https://doi.org/10.1016/j.jnoncrysol.2005.11.042
15. Schreurs J.W., Brill R.H.: Iron and sulfur related colors in ancient glasses, Archaeometry 26(2), 1984, pp. 199-209. https://doi.org/10.1111/j.1475-4754.1984.tb00334.x
16. Bacon F.R., Billian C.J.: Color and spectral transmittance of amber bottle glass, J. Am. Ceram. Soc. 37(2), 1954, pp. 60-66. https://doi.org/10.1111/j.1151-2916.1954.tb14006.x
17. Dhand V., Mittal G., Rhee K.Y., et al.: A short review on basalt fiber reinforced polymer composites, Compos. Part B-Eng. 73, 2015, pp. 166-180. https://doi.org/10.1016/j.compositesb.2014.12.011
18. Khandelwal S., Rhee K.Y.: Recent advances in basalt-fiber-reinforced composites: Tailoring the fiber-matrix interface. Compos. Part B-Eng. 192, 2020, 108011 p. https://doi.org/10.1016/j.compositesb.2020.108011
19. Hao L., Yu W.: Evaluation of thermal protective performance of basalt fiber nonwoven fabrics, J. Thermal Anal. Calor. 100(2), 2010, pp. 551-555. https://doi.org/10.1007/s10973-009-0179-0
20. Moiseev E.A., Gutnikov S.I., Malakho A.P., et al.: Effect of iron oxides on the fabrication and properties of continuous glass fibers, Inorg. Mater. 44, 2008, pp. 1026–1030. https://doi.org/10.1134/S0020168508090215
21. Gutnikov S.I., Manylov M.S., Lipatov Ya.V., et al.: Effect of the reduction treatment on the basalt continuous fiber crystallization properties, J. Non-Cryst. Solids 368, 2013, pp. 45–50. https://doi.org/10.1016/j.jnoncrysol.2013.03.007
22. Gutnikov S.I., Manylov M.S., Lazoryak B.I.: Crystallization and thermal stability of the P-doped basaltic glass fibers. Minerals 9(10), 2019, pp. 615. https://doi.org/10.3390/min9100615
23. Overkamp T., Mahltig B., Kyosev Y.: Strength of basalt fibers influenced by thermal and chemical treatments. J. Ind. Text. 47(5), 2018, pp. 815-833. https://doi.org/10.1177/1528083716674905.x
24. Fiore V., Scalici T., Di Bella G., et al.: A review on basalt fibre and its composites, Compos. Part B-Eng. 74, 2015, pp. 74–94. https://doi.org/10.1016/j.compositesb.2014.12.034
25. Lipatov Y.V., Arkhangelsky I.V., Dunaev A.V., et al.: Crystallization of zirconia doped basalt fibers, Thermochim. Acta 575, 2014, pp. 238–243. https://doi.org/10.1016/j.tca.2013.11.002
26. Bunker G.: Introduction to XAFS, Cambridge University Press, 2010.
27. Calvin S.: XAFS for Everyone, CRC Press, 2013.
28. Newville M.: Fundamentals of XAFS, Rev. Mineral. Geochem.78 (1), 2014, pp. 33–74. https://doi.org/10.2138/rmg.2014.78.2
29. Sharma S.K., Verma D.S. (ed.): Handbook of materials characterization, Cham: Springer, chapter 13, 2018.
30. D'Amico S., Venuti V. (ed.): Handbook of cultural heritage analysis, Cham: Springer (Springer nature reference), 2022.
31. Gates W.P., Bergaya F., Theng B.K.G., et al. (ed.): X-ray absorption spectroscopy, Handbook of Clay Science, Chapter 12.3, Developments in clay science 1, 2006, pp. 789 – 864.
32. Buzanich A.G.: Recent developments of X-ray absorption spectroscopy as analytical tool for biological and biomedical applications, X-Ray Spectrom. 51(3), 2022, pp. 294–303. https://doi.org/10.1002/xrs.3254
33. Iglesias-Juez A., Chiarello G.L., Patience G.S., et al.: Experimental methods in chemical engineering: X-ray absorption spectroscopy — XAS, XANES, EXAFS. Can. J. Chem. Eng. 100(1), 2022, pp. 3–22. https://doi.org/10.1002/cjce.24291
34. Iwasawa Y., Asakura K., Tada M. (ed.): XAFS techniques for catalysts, nanomaterials, and surfaces, Cham: Springer International Publishing, 2017, online: http://dx.doi.org/10.1007/978-3-319-43866-5
35. Prange A., Modrow H.: X-ray absorption spectroscopy and its application in biological, agricultural and environmental research., Rev. Environ. Sci. Bio. 1(4), 2002, pp. 259–276. https://doi.org/10.1023/A:1023281303220
36. Mahltig B.: High-performance fibres – A review of properties and IR-spectra, Tekstilec 64, 2021, pp. 96-118. https://doi.org/10.14502/Tekstilec2021.64.96-118
37. Mahltig B., Grethe T.: High-performance and functional fiber materials—A review of properties, scanning electron microscopy SEM and electron dispersive spectroscopy EDS, Textiles 2, 2022, pp. 209-252. https://doi.org/10.3390/textiles2020012
38. Ruffen C., Mahltig B.: Basalt fibers as functional additives in coating of textiles, J. Coat. Technol. Res. 18, 2021, pp. 271-281. https://doi.org/10.1007/s11998-020-00383-8
39. Klysubun W., Sombunchoo P., Wongprachanukul N., et al.: Commissioning and performance of X-ray absorption spectroscopy beamline at the Siam Photon Laboratory, Nucl. Instrum. Meth. A 582, 2007, pp. 87–89. https://doi.org/10.1016/j.nima.2007.08.067
40. Klysubun W., Tarawarakarn P., Thamsanong N., et al.: Upgrade of SLRI BL8 beamline for XAFS spectroscopy in a photon energy range of 1–13 keV, Radiat. Phys. Chem. 175, 2020, 108145 p. https://doi.org/10.1016/j.radphyschem.2019.02.004
41. Klysubun W., Sombunchoo P., Deenan W., et al.: Performance and status of beamline BL8 at SLRI for X-ray absorption spectroscopy, J. Synchrotron Radiat. 19, 2012, pp. 930–936. https://doi.org/10.1107/S0909049512040381
42. Cooper R.F., Fanselow J.B., Poker D.B.: The mechanism of oxidation of a basaltic glass: Chemical diffusion of network-modifying cations, Geochim. Cosmochim. Ac. 60(17), 1996, pp. 3253–3265. https://doi.org/10.1016/0016-7037(96)00160-3
43. Yilmaz S., Özkan O.T., Günay V.: Crystallization kinetics of basalt glass, Ceram. Int. 22(6), 1996, pp. 477–481. https://doi.org/10.1016/0272-8842(95)00118-2
44. Morozov N.N., Bakunov V.S., Morozov E.N., et al.: Materials based on basalts from the European north of Russia, Glass Ceram+ 58 (3/4), 2001, pp. 100–104. https://doi.org/10.1023/a:1010947415202
45. Burkhard D.J.M.: Crystallization and oxidation of Kilauea basalt glass: Processes during reheating experiments, J. Petrology 42(3), 2001, pp. 507–527. https://doi.org/10.1093/petrology/42.3.507

46. Chen X., Zhang Y., Hui D., et al.: Study of melting properties of basalt based on their mineral components, Compos. Part B-Eng. 116, 2017, pp. 53–60. https://doi.org/10.1016/j.compositesb.2017.02.014
47. Ravel B., Newville M.: ATHENA, ARTEMIS, HEPHAESTUS: data analysis for X-ray absorption spectroscopy using IFEFFIT, J. Synchrotron Radiat. 12, 2005, pp. 537–541. https://doi.org/10.1107/S0909049505012719
48. Henderson G.S., De Groot F.M.F., Moulton B.J.A.: X-ray absorption near-edge structure (XANES) spectroscopy. Henderson G.S., Neuville D.R., Downs R.T. (ed.): Spectroscopic methods in mineralogy and materials sciences, Boston, Chantilly, Virginia: DE GRUYTER; Mineralogical Society of America, Rev. Mineral. Geochem. 78, 2015, pp. 75–138.
49. Li D., Bancroft G.M., Kasrai M., et al.: X-ray absorption spectroscopy of silicon dioxide ($SiO_2$) polymorphs: The structural characterization of opal, Am. Mineral. 79, 1994, pp. 622–632.
50. Li D., Bancroft G.M., Fleet M.E., et al.: Silicon K-edge XANES spectra of silicate minerals, Phys. Chem. Miner. 22, 1995, pp. 115-122.
51. Gilbert B., Frazer B.H., Naab F., et al.: X-ray absorption spectroscopy of silicates for in situ, sub-micrometer mineral identification, Am. Mineral. 88, 2003, pp. 763–769. https://doi.org/10.2138/am-2003-5-605
52. De Ligny D., Neuville D.R., Cormier L., et al.: Silica polymorphs, glass and melt: An in situ high temperature XAS study at the Si K-edge, J. Non-Cryst. Solids 355, 2009, pp. 1099-1102.
53. Hormes J., Klysubun W., Göttert J., et al.: A new SOLARIS beamline optimized for X-ray spectroscopy in the tender energy range, Nucl. Instrum. Meth. B 489, 2021, pp. 76–81. https://doi.org/10.1016/j.nimb.2020.12.017
54. Davoli I., Paris E., Stizza S., et al.: Structure of densified vitreous silica – silicon and oxygen XANES spectra and multiple-scattering calculations, Phys. Chem. Miner. 19, 1992, pp. 171-175.
55. Henderson G.S., Fleet M.E.: The structure of titanium silicate glasses investigated by Si K-edge X-ray absorption spectroscopy, J. Non-Cryst. Solids 211, 1997, pp. 214-221.
56. De Wispelaere S., Cabaret D., Levelut C., et al.: Na-, Al- and Si K-edge XANES study of sodium silicate and sodium aluminosilicate glasses: influence of the glass surface, Chem. Geol. 213, 2004, pp. 63-70.
57. Cabaret D., Le Grand M., Ramos A., et al.: Medium range structure of borosilicate glasses from Si K-edge XANES: a combined approach based on multiple scattering and molecular dynamics calculations, J. Non-Cryst. Solids 289(1-3), 2001, pp. 1–8. https://doi.org/10.1016/S0022-3093(01)00733-5
58. Militký J., Kovačič V., Rubnerová J.: Influence of thermal treatment on tensile failure of basalt fibers, Eng. Fract. Mech. 69(9), 2002, pp. 1025–1033. https://doi.org/10.1016/S0013-7944(01)00119-9
59. Tamás-Bényei P., Sántha P.: Potential applications of basalt fibre composites in thermal shielding, J. Therm. Anal. Calorim. 148(2), 2023, pp. 271–279. https://doi.org/10.1007/s10973-022-11799-2
60. Cormier L., Neuville D.R.: Ca and Na environments in $Na_2O$–$CaO$–$Al_2O_3$–$SiO_2$ glasses: influence of cation mixing and cation-network interactions, Chem. Geol. 213(1-3), 2004, pp. 103–113. https://doi.org/10.1016/j.chemgeo.2004.08.049
61. Neuville D.R., Cormier L., Flank A.M., et al.: Al speciation and Ca environment in calcium aluminosilicate glasses and crystals by Al and Ca K-edge X-ray absorption spectroscopy, Chem. Geol. 213(1-3), 2004, pp. 153–163. https://doi.org/10.1016/j.chemgeo.2004.08.039
62. Morizet Y., Trcera N., Larre C., et al.: X-ray absorption spectroscopic investigation of the Ca and Mg environments in $CO_2$-bearing silicate glasses, Chem. Geol. 510, 2019, pp. 91–102. https://doi.org/10.1016/j.chemgeo.2019.02.014
63. Guo X., Wu J., Yiu Y.M., et al.: Drug-nanocarrier interaction–tracking the local structure of calcium silicate upon ibuprofen loading with X-ray absorption near edge structure (XANES), Phys. Chem. Chem. Phys. 15(36), 2013, pp. 15033–15040. https://doi.org/10.1039/c3cp50699a
64. Brinza L., Schofield P.F., Hodson M.E., et al.: Combining μXANES and μXRD mapping to analyse the heterogeneity in calcium carbonate granules excreted by the earthworm Lumbricus terrestris, J. Synchrotron Radiat. 21(Pt 1), 2014, pp. 235–241. https://doi.org/10.1107/S160057751303083X
65. Kathyola T.A., Chang S.Y., Willneff E.A., et al.: X-ray absorption spectroscopy as a process analytical technology: Reaction studies for the manufacture of sulfonate-stabilized calcium carbonate particles, Indu. Eng. Chem. Res. 62(40), 2023, pp. 16198–16206. https://doi.org/10.1021/acs.iecr.3c02540
66. Monico L., Cartechini L., Rosi F., et al.: Synchrotron radiation Ca K-edge 2D-XANES spectroscopy for studying the stratigraphic distribution of calcium-based consolidants applied in limestones, Scientific Reports 10(1), 2020, pp. 14337. https://doi.org/10.1038/s41598-020-71105-8
67. Xto J., Wetter R., Borca C.N., et al.: Droplet-based in situ X-ray absorption spectroscopy cell for studying crystallization processes at the tender X-ray energy range, RSC Adv. 9(58), 2019, pp. 34004–34010. https://doi.org/10.1039/c9ra06084g
68. Levi-Kalisman Y., Raz S., Weiner S., et al.: X-Ray absorption spectroscopy studies on the structure of a biogenic “amorphous” calcium carbonate phase, J. Chem. Soc. Dalton Trans. (21), 2000, pp. 3977–3982. https://doi.org/10.1039/B003242P
69. Levi-Kalisman Y., Raz S., Weiner S., et al.: Structural differences between biogenic amorphous calcium carbonate phases using X-ray absorption spectroscopy. Adv. Funct. Mater. 12(1), 2002, pp. 43. https://doi.org/10.1002/1616-3028(20020101)12:1%3C43::AID-ADFM43%3E3.0.CO;2-C
70. Lam R.S.K., Charnock J.M., Lennie A., et al.: Synthesis-dependant structural variations in amorphous calcium carbonate, CrystEngComm 9(12), 2007, 1226 p. https://doi.org/10.1039/b710895h
71. Fiege A., Ruprecht P., Simon A.C., et al.: Calibration of Fe XANES for high-precision determination of Fe oxidation state in glasses: Comparison of new and existing results obtained at different synchrotron radiation sources, Am. Mineral. 102(2), 2017, pp. 369-380. https://doi.org/10.2138/am-2017-5822
72. Cottrell E., Kelley K.A., Lanzirotti A., et al.: High-precision determination of iron oxidation state in silicate glasses using XANES, Chem. Geol. 268(3-4), 2009, pp. 167-179. https://doi.org/10.1016/j.chemgeo.2009.08.008
73. Wilke M., Farges F., Petit P.E., et al.: Oxidation state and coordination of Fe in minerals: An Fe K- XANES spectroscopic study, Am. Mineral. 86(5-6), 2001, pp. 714–730. https://doi.org/10.2138/am-2001-5-612
74. Westre T.E., Kennepohl P., DeWitt J.G., et al.: A multiplet analysis of Fe K-Edge 1s → 3d pre-edge features of iron complexes, J. Am. Chem. Soc. 119(27), 1997, pp. 6297–6314. https://doi.org/10.1021/ja964352a
75. Boubnov A., Lichtenberg H., Mangold S., et al.: Identification of the iron oxidation state and coordination geometry in iron oxide- and zeolite-based catalysts using pre-edge XAS analysis, J. Synchrotron Radiat. 22(2), 2015, pp. 410–426. https://doi.org/10.1107/S1600577514025880